

Perturbative quantum Monte Carlo method for nuclear physics

Bing-Nan Lu,^{1,*} Ning Li,² Serdar Elhatisari,³ Yuan-Zhuo Ma,⁴ Dean Lee,^{5,†} and Ulf-G. Meißner^{6,7,8,‡}

¹Graduate School of China Academy of Engineering Physics, Beijing 100193, China

²School of Physics, Sun Yat-Sen University, Guangzhou 510275, China

³Faculty of Natural Sciences and Engineering, Gaziantep Islam Science and Technology University, Gaziantep 27010, Turkey

⁴Guangdong Provincial Key Laboratory of Nuclear Science, Institute of Quantum Matter, South China Normal University, Guangzhou 510006, China

⁵Facility for Rare Isotope Beams and Department of Physics and Astronomy, Michigan State University, MI 48824, USA

⁶Helmholtz-Institut für Strahlen- und Kernphysik and Bethe Center for Theoretical Physics, Universität Bonn, D-53115 Bonn, Germany

⁷Institute for Advanced Simulation, Institut für Kernphysik, and Jülich Center for Hadron Physics,

Forschungszentrum Jülich, D-52425 Jülich, Germany

⁸Tbilisi State University, 0186 Tbilisi, Georgia

While first order perturbation theory is routinely used in quantum Monte Carlo (QMC) calculations, higher-order terms present significant numerical challenges. We present a new approach for computing perturbative corrections in projection QMC calculations. We demonstrate the method by computing nuclear ground state energies up to second order for a realistic chiral interaction. We calculate the binding energies of several light nuclei up to ^{16}O by expanding the Hamiltonian around the Wigner SU(4) limit and find good agreement with data. In contrast to the natural ordering of the perturbative series, we find remarkably large second order energy corrections. This occurs because the perturbing interactions break the symmetries of the unperturbed Hamiltonian. Our method is free from the sign problem and can be applied to QMC calculations for many-body systems in nuclear physics, condensed matter physics, ultracold atoms, and quantum chemistry.

Quantum Monte Carlo (QMC) simulation is a powerful method for addressing quantum many-body problems in nuclear physics [1–4], condensed matter [5–7], ultracold atoms [8–10], and quantum chemistry [11, 12]. Perhaps the most important feature of QMC is that when the MC process has only positive weights, the computational effort scales only polynomially with system size. Unfortunately, this is not true in general. If the Monte Carlo process involves cancellations between positive and negative weights, the resulting “sign problem” leads to exponential scaling of the computational effort with system size. Although finding a generic solution for the sign problem is unlikely in the near term [13], for several important cases QMC algorithms can be applied without sign problems, such as lattice QCD at zero baryon density [14], the repulsive Fermi-Hubbard model at half-filling [15], and low-energy nuclear systems in the Wigner SU(4) limit [1, 16, 17, 19]. The realistic systems of physical interests, though, often deviate from these ideal models significantly and have a sign problem. In these cases, perturbation theory can be used to bridge the difference between the simplified and the realistic interaction. However, so far perturbation theory in QMC is mostly limited to the first order. Improving the quality of the perturbative calculations requires going to higher orders.

In Rayleigh-Schrödinger perturbation theory, the second-order energy correction involves a summation over all quantum states that can be reached via the perturbing interaction. Such a calculation over all quantum states is not compatible with QMC, which targets only the lowest energy states. To solve this problem, we introduce a computational framework called perturbative QMC (ptQMC), which allows for the efficient calculation of higher-order perturbative corrections within the Euclidean time formalism. As a demonstration, we implement this method using nuclear lattice effective field

theory (NLEFT) [3, 4] and perform benchmark calculations of the binding energies of several nuclei.

NLEFT is a QMC method for nuclear *ab initio* calculations. We regularize the chiral nuclear force on a periodic cubic lattice and employ the auxiliary field MC method to simulate finite nuclei. The advantage of this approach is that many-body correlation effects such as clustering emerge automatically [22, 23]. Due to the sign problem, early NLEFT calculations were limited to a few nuclei and specially designed interactions [24–29]. In most of the recent NLEFT calculations, the higher order chiral interactions are included with first order perturbation theory [30–34].

The nuclear Hamiltonian is $H = K + V_0 + V_C$, with $K = -\nabla^2/2m$ the kinetic energy operator and $m = 938.92$ MeV the nucleon mass. We use a lattice spacing of $a = 1.32$ fm. The interaction is split into a dominant term V_0 and a correction V_C . The ground state of H can be found by applying imaginary time projectors to a trial wave function $|\Psi_T\rangle$, $|\Psi\rangle = \lim_{L_t \rightarrow \infty} M^{L_t/2} |\Psi_T\rangle$, with $M =: e^{-a_t H}$: the transfer matrix and a_t the temporal step. The colons denote normal ordering. Without loss of generality, we assume that both V_0 and V_C can be decomposed in terms of auxiliary fields. For example, using a simple contact interaction for V_0 ,

$$: e^{-\frac{1}{2}a_t C_0 \rho(\mathbf{n})^2} : \propto \int \mathcal{D}s : e^{-\frac{s(\mathbf{n})^2}{2} + \sqrt{-a_t C_0} s(\mathbf{n}) \rho(\mathbf{n})} :, \quad (1)$$

with $\rho(\mathbf{n})$ the nucleon density and $s(\mathbf{n})$ a real auxiliary field. We further require that V_0 does not induce a sign problem. This is possible when V_0 is attractive with $C_0 < 0$, and each spin-up nucleon in $|\Psi_T\rangle$ is paired with a spin-down nucleon [35]. This is the case for the ground states of even-even nuclei. However, we can use a more general V_C that may have a sign problem. By decomposing V_C in the same manner, we have similar expressions for the density ρ_c and the corresponding

auxiliary field c . For non-perturbative QMC calculations, we need to sample both s and c fields.

Under the assumption that V_C is small compared to V_0 , we can expand $|\Psi\rangle$ in powers of V_C ,

$$|\Psi\rangle = \lim_{L_t \rightarrow \infty} M^{L_t/2} |\Psi_T\rangle = |\Psi_0\rangle + |\delta\Psi_1\rangle + \mathcal{O}(V_C^2), \quad (2)$$

$$|\Psi_0\rangle = \lim_{L_t \rightarrow \infty} M_0^{L_t/2} |\Psi_T\rangle, \quad (3)$$

$$|\delta\Psi_1\rangle = \lim_{L_t \rightarrow \infty} \sum_{k=1}^{L_t/2} M_0^{L_t/2-k} (M - M_0) M_0^{k-1} |\Psi_T\rangle, \quad (4)$$

where $M_0 =: e^{-a_t(K+V_0)}$ is the zeroth order transfer matrix and we have omitted the $\mathcal{O}(a_t^2)$ terms. In Eq. (2) and what follows, we use the subscripts to denote the perturbative orders and the symbols with δ to represent the corrections. The normalized wave function is

$$|\Psi'\rangle = \frac{|\Psi\rangle}{\sqrt{\langle\Psi|\Psi\rangle}} = \frac{|\Psi_0\rangle}{\sqrt{\langle\Psi_0|\Psi_0\rangle}} + \frac{1}{\sqrt{\langle\Psi_0|\Psi_0\rangle}} \times \left[|\delta\Psi_1\rangle - \frac{\text{Re}\langle\Psi_0|\delta\Psi_1\rangle}{\langle\Psi_0|\Psi_0\rangle} |\Psi_0\rangle \right] + \mathcal{O}(V_C^2), \quad (5)$$

where Re denotes the real part. Eq. (5) can be used to calculate the expectation value of any operator up to $\mathcal{O}(V_C)$. A special case is the energy, for which δE_1 only depends on $|\Psi_0\rangle$. With $|\delta\Psi_1\rangle$ at hand, we can continue further to find δE_2 . The partial energy contributions at each order are

$$E_0 = \langle\Psi_0|(K + V_0)|\Psi_0\rangle / \langle\Psi_0|\Psi_0\rangle, \quad (6)$$

$$\delta E_1 = \langle\Psi_0|V_C|\Psi_0\rangle / \langle\Psi_0|\Psi_0\rangle, \quad (7)$$

$$\delta E_2 = \text{Re}(\langle\Psi_0|V_C|\delta\Psi_1\rangle - \delta E_1 \langle\Psi_0|\delta\Psi_1\rangle) / \langle\Psi_0|\Psi_0\rangle, \quad (8)$$

where all matrix elements and overlaps can be expressed with the amplitudes,

$$\mathcal{M}(O) = \langle\Psi_T|M_0^{L_t/2} O M_0^{L_t/2} |\Psi_T\rangle, \quad (9)$$

$$\mathcal{M}_k(O) = \langle\Psi_T|M_0^{L_t/2} O M_0^{L_t/2-k} M M_0^{k-1} |\Psi_T\rangle, \quad (10)$$

where $k = 1, 2, \dots, L_t/2$. Here O is the operator inserted in the middle time step like $1, K + V_0$ or V_C . In $\mathcal{M}_k(O)$ the k -th copy of M_0 is replaced by the full transfer matrix M . The transfer matrices M_0 and M in these amplitudes are computed using the auxiliary field formalism.

The energies E_0 and δE_1 are just the expectation values $\langle O \rangle = \mathcal{M}(O) / \mathcal{M}(1)$ with $O = K + V_0$ or V_C . These can be calculated by sampling the auxiliary fields s in M_0 with standard algorithms [3, 4]. For δE_2 we need to evaluate an integral over the auxiliary field c from the inserted M in $\mathcal{M}_k(O)$. For every sample $\{s_1, s_2, \dots, s_{L_t}\}$ we have

$$\mathcal{M}_k(O) = \int \mathcal{D}c P(c+\bar{c}) \langle \dots O \dots M(s_k, c+\bar{c}) \dots \rangle_T, \quad (11)$$

where the ellipses denote the transfer matrices $M_0(s_t)$ with $t \neq k$, $\langle \rangle_T$ the expectation value in the state $|\Psi_T\rangle$ and $P(c)$ is the standard normal distribution. In Eq. (11) we have made a

variable change $c \rightarrow \bar{c} + c$ with c real integral variables. Here $\bar{c}(\mathbf{n})$ is a constant field

$$\begin{aligned} \bar{c}(\mathbf{n}) &= \frac{\partial}{\partial c(\mathbf{n})} \ln \langle \dots M(s_k, c) \dots \rangle_T \Big|_{c=0} \\ &= \sqrt{-a_t C} \langle \dots : M_0(s_k) \rho_c(\mathbf{n}) : \dots \rangle_T / \mathcal{M}(1), \end{aligned} \quad (12)$$

where the ellipses again represent the M_0 's, C is the coupling constant for the V_C term. Generally, \bar{c} is a complex field, e.g., for repulsive interactions such as Coulomb we have $C > 0$, the square root in Eq. (12) introduces an imaginary factor i . In this case the integrand in Eq. (11) contains non-zero phases that may induce a severe sign problem. The variable change in Eq. (11) serves to alleviate this problem [36]. To see this, we take the logarithm of the integrand in Eq. (11), expand the result near $c = 0$ and apply Eq. (12). We find that the terms linear in c and \bar{c} which cause the sign problem cancel exactly and the integrand can be factorized as

$$\mathcal{M}_k(O) = \mathcal{M}(s) \exp\left(\frac{\bar{c}^2}{2}\right) \int \mathcal{D}c \exp\left(-\frac{c^2}{2} + \epsilon\right), \quad (13)$$

where we omit the summations over lattice sites, ϵ is a residual term containing quadratic and higher powers of c . Because in $\mathcal{M}_k(s, c)$ a common factor $\sqrt{a_t}$ is attached to every c variable, ϵ is a small number of the order $\mathcal{O}(a_t)$. For sufficiently small a_t , Eq. (13) means that the integrand in Eq. (11) is a product of a normal distribution and a slowly varying function $\exp(\epsilon)$. We can use stochastic methods to evaluate Eq. (11) by sampling the c field with a standard normal distribution. This evaluation is unbiased and its uncertainty is determined by the variation of $\exp(\epsilon)$. In practice, we found that the variable change in Eq. (11) can reduce the statistical error by one order or more, see [37] for a demonstration.

We benchmark the ptQMC using a realistic nuclear chiral force with two-body and three-body interactions up to N²LO [21, 38]. The two-body contact terms and the one-pion-exchange potential (OPEP) read

$$\begin{aligned} V_{2N} &= [B_1 + B_2(\boldsymbol{\sigma}_1 \cdot \boldsymbol{\sigma}_2) + C_1 q^2 + C_2 q^2 (\boldsymbol{\tau}_1 \cdot \boldsymbol{\tau}_2) \\ &+ C_3 q^2 (\boldsymbol{\sigma}_1 \cdot \boldsymbol{\sigma}_2) + C_4 q^2 (\boldsymbol{\sigma}_1 \cdot \boldsymbol{\sigma}_2) (\boldsymbol{\tau}_1 \cdot \boldsymbol{\tau}_2) \\ &+ C_5 \frac{i}{2} (\mathbf{q} \times \mathbf{k}) \cdot (\boldsymbol{\sigma}_1 + \boldsymbol{\sigma}_2) + C_6 (\boldsymbol{\sigma}_1 \cdot \mathbf{q}) (\boldsymbol{\sigma}_2 \cdot \mathbf{q}) \\ &+ C_7 (\boldsymbol{\sigma}_1 \cdot \mathbf{q}) (\boldsymbol{\sigma}_2 \cdot \mathbf{q}) (\boldsymbol{\tau}_1 \cdot \boldsymbol{\tau}_2)] f_{2N}(p_1, p_2, p'_1, p'_2) \\ &- \frac{g_A^2 f_\pi(q^2)}{4F_\pi^2} \left[\frac{(\boldsymbol{\sigma}_1 \cdot \mathbf{q}) (\boldsymbol{\sigma}_2 \cdot \mathbf{q})}{q^2 + M_\pi^2} + C'_\pi \boldsymbol{\sigma}_1 \cdot \boldsymbol{\sigma}_2 \right] (\boldsymbol{\tau}_1 \cdot \boldsymbol{\tau}_2), \end{aligned} \quad (14)$$

where $\boldsymbol{\sigma}_{1,2}(\boldsymbol{\tau}_{1,2})$ are spin (isospin) matrices, B_i, C_i are low-energy constants (LECs). \mathbf{p} and \mathbf{p}' are the relative incoming and outgoing momenta, respectively, $\mathbf{q} = \mathbf{p} - \mathbf{p}'$, $\mathbf{k} = (\mathbf{p} + \mathbf{p}')/2$ are momentum transfers, \mathbf{p}_i and \mathbf{p}'_i are the momenta of the individual nucleons, g_A, F_π, M_π are the axial-vector coupling constant, pion decay constant and pion mass, respectively. The additional regulators, $f_{2N} = \exp[-\sum_{i=1}^2 (p_i^6 + p_i'^6) / \Lambda^6]$ with $\Lambda = 340$ MeV and $f_\pi =$

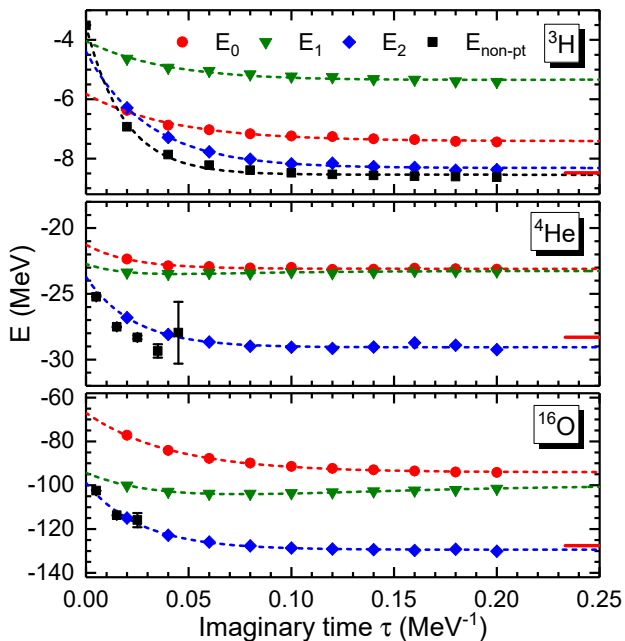


Figure 1. ptQMC binding energies as functions of the projection time τ compared with non-perturbative results. The circles (red), down triangles (green) and diamonds (blue) denote the energies at the zeroth, first and second orders, respectively. The squares (black) represent the exact results calculated with sparse matrix multiplications for ${}^3\text{H}$ and full non-perturbative QMC for ${}^4\text{He}$ and ${}^{16}\text{O}$, respectively. Each group of results are fitted with a sum of exponential functions (dashed lines). The red bars mark the experimental binding energies.

$\exp[-(q^2 + M_\pi^2)/\Lambda_\pi^2]$ with $\Lambda_\pi = 300$ MeV, are introduced to minimize lattice artifacts. For the OPEP we introduce a counterterm $\sim C'_\pi$ as in Ref. [38] to remove the short-range singularity, which, together with a low Λ_π , adapts the potential to perturbative calculations. Note that the OPEP contains a tensor interaction that couples different partial waves, thus will contribute significantly to the energy at second order. For the three-body force V_{3N} we adopt a simple 3N contact term with the LEC c_E . The LECs B_i, C_i, c_E are fixed from NN scattering data and the triton binding energy. We also implement a static Coulomb force V_{cou} , see [37] for further details of the interaction.

In order to compute ground states of $H = K + V_{2N} + V_{3N} + V_{\text{cou}}$ using ptQMC, we shall choose a zeroth order Hamiltonian $H_0 = K + V_0$ and calculate the energy corrections with respect to $V_C = H - H_0$. We take V_0 to be the non-locally smeared SU(4) interaction from Ref. [1], which captures the essential elements of the nuclear force. For benchmarking purposes, we only keep the two-body part of V_0 , which induces no sign problem for even-even nuclei. The details of V_0 can be found in [37]. For further work starting with the Wigner SU(4) limit, see [39–41].

In Fig. 1 we compare the results obtained using ptQMC with non-perturbative results. We use a periodic box of size $L = 10$ for ${}^3\text{H}$ and $L = 8$ for the other nuclei. The temporal step is $a_t = 1/1000$ MeV $^{-1}$. For ${}^3\text{H}$, the system is small

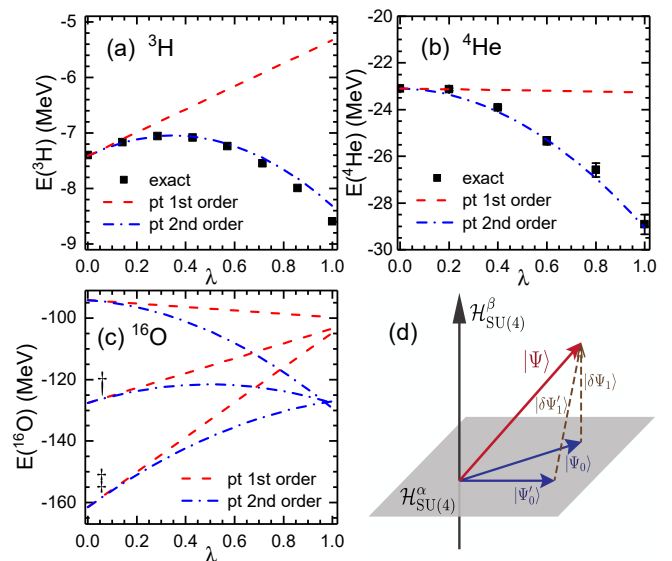


Figure 2. (a)(b) The dashed and dash-dotted lines denote the binding energies of ${}^3\text{H}$ (a) and ${}^4\text{He}$ (b) as functions of the small parameter λ in first and second order ptQMC calculations, respectively. The black squares are the exact results. (c) The first and second order ptQMC calculations for ${}^{16}\text{O}$, starting from three different perturbation interactions $V_0, 1.1V_0$ (\dagger) and $1.2V_0$ (\ddagger). (d) Schematic plot for a perturbative calculation. The zeroth order wave functions $|\Psi_0\rangle$ and $|\Psi'_0\rangle$ are confined in a subspace corresponding to an *irrep* of SU(4).

enough that we can use exact sparse matrix calculations. For larger nuclei we perform fully non-perturbative QMC calculations instead, which result in large error bars due to severe sign problems. For the ${}^{16}\text{O}$ nucleus, the sign problem sets in so quickly that we cannot find meaningful results to make a reliable extrapolation. However, the ptQMC calculations are free from sign problems. The corresponding statistical errors are smaller than the size of the symbols. We use a sum of decaying exponential functions to capture the residual effects of higher energy excitations and extrapolate the results to $\tau \rightarrow \infty$. See [37] for further settings of the QMC simulation. For all three nuclei, the second order energy corrections are large and essential in reproducing the data. While this might seem contrary to the normal hierarchy of the perturbative series, we will show below that it is actually a consequence of the symmetry breaking.

We can now examine the convergence pattern of the perturbative series. In Fig. 2(a)(b)(c) we show the calculated energies as a function of λ , a real number between 0 and 1 that we insert as a control parameter multiplying the perturbation V_C . The ptQMC results are shown as lines. Because ptQMC corresponds to the Taylor series expansion at $\lambda = 0$, we find straight lines at first and parabolas at second order. For ${}^3\text{H}$ (${}^4\text{He}$) we also display the exact energies of $H_0 + \lambda V_C$ obtained with sparse matrix diagonalization. The difference between the second order and exact results indicate the contributions from the third and higher orders, which are more than one order smaller in magnitude.

Table I. Binding energies at different orders calculated with ptQMC, compared to experiment (all in MeV). The errors are combinations of MC statistical errors and extrapolation errors [37]. See Fig. 2(c) for further notations.

	E_0	δE_1	E_1	δE_2	E_2	E_{exp}
^3H	-7.41(3)	+2.08	-5.33(3)	-2.99	-8.32(3)	-8.48
^4He	-23.1(0)	-0.2	-23.3(0)	-5.8	-29.1(1)	-28.3
^8Be	-44.9(4)	-1.7	-46.6(4)	-11.1	-57.7(4)	-56.5
^{12}C	-68.3(4)	-1.8	-70.1(4)	-18.8	-88.9(3)	-92.2
^{16}O	-94.1(2)	-5.6	-99.7(2)	-29.7	-129.4(2)	-127.6
$^{16}\text{O}^\dagger$	-127.6(4)	+24.2	-103.4(4)	-24.3	-127.7(2)	-127.6
$^{16}\text{O}^\ddagger$	-161.5(1)	+56.8	-104.7(2)	-22.3	-127.0(2)	-127.6

For ^{16}O we cannot obtain non-perturbative results for benchmarking due to the severe sign problem, and so instead we vary the zeroth order Hamiltonian to triangulate the binding energy and estimate its uncertainty. In Fig. 2(c) the \dagger and \ddagger symbols mark the ptQMC energies calculated with $H_0 = K + 1.1V_0$ and $H_0 = K + 1.2V_0$, respectively. For each calculation, we use $V_C = H - H_0$ as the perturbing Hamiltonian and plot the energies as functions of the small parameter λ . While the variation of H_0 shifts the zeroth order energy by about 50 MeV, for full Hamiltonian H ($\lambda = 1$) we find that the first and second order energies only vary by about 4 MeV and 2.4 MeV, respectively. These variations can be identified as the truncation errors of the perturbative series at corresponding orders, see also [37].

In Tab. I we present the ptQMC energies for several nuclei compared to the empirical values. The improvement of E_2 compared with E_1 is clearly seen. Generally, the correlation energy δE_2 accounts for about 20% of the total binding energy for all nuclei with $A \geq 4$. We note that the first order energy is the expectation value of the full Hamiltonian using the zeroth order wave function $|\Psi_0\rangle$, and it is an upper bound on the ground state energy. The energy correction δE_2 is negative definite, reflecting the fact that the corrected wave function $|\Psi_1\rangle$ is much closer to the exact ground state than $|\Psi_0\rangle$.

In perturbative calculations the convergence pattern can be invalidated by symmetry constraints. As the unperturbed Hamiltonian H_0 respects the SU(4) symmetry, the wave function $|\Psi_0\rangle$ must belong to one of its irreducible representations (*irreps*). The full Hamiltonian breaks the SU(4) symmetry, thus its ground state $|\Psi\rangle$ is a mixture of different SU(4) *irreps*. As is shown in Fig. 2(d), the components of $|\Psi\rangle$ that mixes the SU(4) *irreps* can only be seen in $|\delta\Psi_1\rangle$ or δE_2 . This explains the large δE_2 in ^{16}O that can not be eliminated by varying H_0 . We note that this effect is strongest for the OPEP in Eq. (14) as it breaks both the Wigner-SU(4) and the spin SU(2) symmetries.

In summary, we have presented a novel algorithm (ptQMC) that allows for a precise calculation of the second order perturbative correction in QMC without referring to the full spectrum of the excited states. While the QMC method with simplified interactions are successfully applied in various fields

of physics [1, 44–54], attempts to use more realistic interactions are hindered by the sign problem. The ptQMC method is free from sign problems and opens the way to treat complex interactions systematically. Our method converges quickly for relatively soft interactions. For interactions with strong short-distance correlations such as tensor forces, which are important in electroweak processes [55], some pre-processing of the interaction using renormalization group transformations or some analogous method is required.

Acknowledgements We are grateful for discussions with members of the Nuclear Lattice Effective Field Theory Collaboration. We gratefully acknowledge funding by NSAF (Grant No. U1930403), the Deutsche Forschungsgemeinschaft (DFG, German Research Foundation) and the NSFC through the funds provided to the Sino-German Collaborative Research Center TRR110 ‘‘Symmetries and the Emergence of Structure in QCD’’ (DFG Project ID 196253076 - TRR 110, NSFC Grant No. 12070131001), the Chinese Academy of Sciences (CAS) President’s International Fellowship Initiative (PIFI) (Grant No. 2018DM0034), Volkswagen Stiftung (Grant No. 93562), the European Research Council (ERC) under the European Union’s Horizon 2020 research and innovation programme (grant agreement No. 101018170) and the U.S. Department of Energy (DE-SC0013365 and DE-SC0021152) and the Nuclear Computational Low-Energy Initiative (NUCLEI) SciDAC-4 project (DE-SC0018083) and the Scientific and Technological Research Council of Turkey (TUBITAK project no. 120F341) and the National Natural Science Foundation of China under Grants No. 12105106 and the China Postdoctoral Science Foundation under Grant No. BX20200136, 2020M682747 as well as computational resources provided by the Beijing Super Cloud Computing Center (BSCC, <http://www.blsc.cn/>), TianHe 3F, the Gauss Centre for Supercomputing e.V. (www.gauss-centre.eu) for computing time on the GCS Supercomputer JUWELS at Jülich Supercomputing Centre (JSC) and the Oak Ridge Leadership Computing Facility through the INCITE award ‘‘Ab-initio nuclear structure and nuclear reactions’’. Further computational resources from the JSC on JURECA DC are gratefully acknowledged.

* bnlv@gscaep.ac.cn

† lee.dean.j@gmail.com

‡ meissner@hiskp.uni-bonn.de

- [1] K. Langanke, D. J. Dean, P. B. Radha, Y. Alhassid and S. E. Koonin, Phys. Rev. C **52**, 718-725 (1995).
- [2] J. Carlson, S. Gandolfi, F. Pederiva, Steven C. Pieper, R. Schiavilla, K. E. Schmidt, and R. B. Wiringa, Rev. Mod. Phys. **87**, 1067 (2015).
- [3] D. Lee, Prog. Part. Nucl. Phys. **63**, 117 (2009).
- [4] T. A. Lähde and U.-G. Meißner, Lect. Notes Phys. **957**, 1-396 (2019).
- [5] D. M. Ceperley and B. J. Alder, Phys. Rev. Lett. **45**, 566-569 (1980).

- [6] W. M. C. Foulkes, L. Mitas, R. J. Needs, and G. Rajagopal, *Rev. Mod. Phys.* **73**, 33 (2001).
- [7] F. F. Assaad and I. F. Herbut, *Phys. Rev. X* **3**, 031010 (2013).
- [8] A. Bulgac, J. E. Drut and P. Magierski, *Phys. Rev. A* **78**, 023625 (2008) doi:10.1103/PhysRevA.78.023625.
- [9] J. Carlson, S. Gandolfi, K. E. Schmidt and S. Zhang, *Phys. Rev. A* **84**, 061602 (2011).
- [10] R. He, N. Li, B. N. Lu and D. Lee, *Phys. Rev. A* **101**, no.6, 063615 (2020).
- [11] B. J. Hammond, W. A. Lester, and P. J. Reynolds (1994), *Monte Carlo Methods in Ab Initio Quantum Chemistry* (World Scientific, Singapore).
- [12] M. Nightingale and C. Umrigar (1999), *Quantum Monte Carlo Methods in Physics and Chemistry* (Springer). NNDC, (2014), “Nudat 2,” <http://www.nndc.bnl.gov/nudat2/chartNuc.jsp>.
- [13] M. Troyer, U.-J. Wiese, *Phys. Rev. Lett* **94**, 170201 (2005).
- [14] S. Muroya, A. Nakamura, C. Nonaka, T. Takaishi, *Prog. Theo. Phys.* **110**, 615 (2003).
- [15] C. N. Varney, C.-R. Lee, Z. J. Bai, S. Chiesa, M. Jarrell, and R. T. Scalettar, *Phys. Rev. B* **80**, 075116 (2009).
- [16] E. Wigner, *Phys. Rev.* **51**, 106 (1937).
- [17] S. Elhatisari, N. Li, A. Rokash, J. M. Alarcon, D. Du, N. Klein, B.-N. Lu, U.-G. Meißner, E. Epelbaum, H. Krebs, T. A. Lähde, D. Lee and G. Rupak, *Phys. Rev. Lett.* **117**, 132501 (2016).
- [18] B.-N. Lu, N. Li, S. Elhatisari, D. Lee, E. Epelbaum, U.-G. Meißner, *Phys. Rev. Lett.* **B 797**, 134863 (2019).
- [19] D. Lee, S. Bogner, B. A. Brown, S. Elhatisari, E. Epelbaum, H. Hergert, M. Hjorth-Jensen, H. Krebs, N. Li, B.-N. Lu, and U.-G. Meißner, *Phys. Rev. Lett.* **127**, 062501 (2021).
- [20] P. Schwerdtfeger, *Chem. Phys. Chem.* **12**, 3143 (2011).
- [21] E. Epelbaum, H.-W. Hammer, and U.-G. Meißner, *Rev. Mod. Phys.* **81**, 1773 (2009).
- [22] S. Elhatisari, E. Epelbaum, H. Krebs, T. A. Lähde, D. Lee, N. Li, B.-N. Lu, U.-G. Meißner, G. Rupak, *Phys. Rev. Lett.* **119**, 222505 (2017).
- [23] N. Summerfield, B.-N. Lu, C. Plumberg, D. Lee, J. Noronha-Hostler, A. Timmins, *Phys. Rev. C* **104**, 041901 (2021).
- [24] B. Borasoy, E. Epelbaum, H. Krebs, D. Lee, U.-G. Meißner, *Eur. Phys. J. A* **31**, 105 (2007).
- [25] B. Borasoy, E. Epelbaum, H. Krebs, D. Lee, U.-G. Meißner, *Eur. Phys. J. A* **35**, 343 (2008).
- [26] E. Epelbaum, H. Krebs, D. Lee, U.-G. Meißner, *Eur. Phys. J. A* **41**, 125 (2009).
- [27] E. Epelbaum, H. Krebs, D. Lee, U.-G. Meißner, *Phys. Rev. Lett.* **104**, 142501 (2010).
- [28] E. Epelbaum, H. Krebs, D. Lee, U.-G. Meißner, *Eur. Phys. J. A* **45**, 335 (2010).
- [29] T. A. Lähde, E. Epelbaum, H. Krebs, D. Lee, U.-G. Meißner, G. Rupak, *Phys. Rev. Lett.* **B 732**, 110 (2014).
- [30] E. Epelbaum, H. Krebs, D. Lee, U.-G. Meißner, *Phys. Rev. Lett.* **106**, 192501 (2011).
- [31] E. Epelbaum, H. Krebs, T. Lähde, D. Lee, U.-G. Meißner, *Phys. Rev. Lett.* **109**, 252501 (2012).
- [32] E. Epelbaum, H. Krebs, T. A. Lähde, D. Lee, U.-G. Meißner, *Phys. Rev. Lett.* **110**, 112502 (2013).
- [33] E. Epelbaum, H. Krebs, T. A. Lähde, D. Lee, U.-G. Meißner, G. Rupak, *Phys. Rev. Lett.* **112**, 102501 (2014).
- [34] S. Elhatisari, D. Lee, G. Rupak, E. Epelbaum, H. Krebs, T. A. Lähde, T. Luu, U.-G. Meißner, *Nature* **528**, 111 (2015).
- [35] Z. X. Li, Y. F. Jiang and H. Yao, *Phys. Rev. Lett.* **117**, 267002 (2016).
- [36] S. Zhang and H. Krakauer, *Phys. Rev. Lett.* **90**, 136401.
- [37] See the *Supplemental Material*, which contains details on the interaction, the trial wave functions, the imaginary time extrapolation, details on the perturbative expansion beyond second order and methods to better estimate the theoretical uncertainties;
- [38] P. Reinert, H. Krebs, E. Epelbaum, *Eur. Phys. J. A* **54**, 86 (2018).
- [39] S. König, H. W. Griebhammer, H.-W. Hammer, and U. van Kolck, *Phys. Rev. Lett.* **118**, 202501 (2017).
- [40] S. König, *Eur. Phys. J. A* **56**, 113 (2020).
- [41] J. Vanasse and D. R. Phillips, *Few-Body Syst.* **58**, 26 (2017).
- [42] J. A. Tjon, *Phys. Rev. Lett.* **B 56**, 217 (1975).
- [43] L. Platter, H. W. Hammer and U.-G. Meißner, *Phys. Rev. Lett.* **B 607**, 254 (2005).
- [44] R. B. Wiringa and S. C. Pieper, *Phys. Rev. Lett.* **89**, 182501 (2002).
- [45] A. W. Sandvik, *Phys. Rev. Lett.* **98**, 227202 (2007).
- [46] L. Wang, Y. H. Liu, M. Iazzi, M. Troyer and G. Harcos, *Phys. Rev. Lett.* **115**, 250601 (2015).
- [47] Z. C. Wei, C. J. Wu, Y. Li, S. W. Zhang and T. Xiang, *Phys. Rev. Lett.* **116**, 250601 (2016).
- [48] Z. X. Li, Y. F. Jiang and H. Yao, *Phys. Rev. Lett.* **117**, 267002 (2016).
- [49] C. J. Wu, J. P. Hu and S. C. Zhang, *Phys. Rev. Lett.* **91**, 186402 (2003).
- [50] C. J. Wu and S. C. Zhang, *Phys. Rev. B* **71**, 155115 (2005).
- [51] A. Bulgac, J. E. Drut and P. Magierski, *Phys. Rev. Lett.* **96**, 090404 (2006).
- [52] A. Richie-Halford, J. E. Drut and A. Bulgac, *Phys. Rev. Lett.* **125**, 060403 (2020).
- [53] C. J. Umrigar, J. Toulouse, C. Filippi, S. Sorella and R. G. Hennig, *Phys. Rev. Lett.* **98**, 110201 (2007).
- [54] D. Hangleiter, I. Roth, D. Nagaj and J. Eisert, *Sci. Adv.* **6**, eabb8341 (2020).
- [55] J. Menéndez, D. Gazit and A. Schwenk, *Phys. Rev. Lett.* **107**, 062501 (2011)

SUPPLEMENTAL MATERIAL

In the main text we focus on the perturbative QMC algorithm and its capability of solving realistic *ab initio* nuclear models. Here, we provide more details. In Eq. (11) we claim that the sign problem in integrating the c field can be alleviated by shifting the integral contour, here we present a numerical demonstration. We also give the details of constructing the N²LO chiral force. We further discuss the imaginary time extrapolation. The deuteron binding energy calculation is used to show that even though second order corrections can be sizeable, effects from the third and higher orders can be small (as claimed in the main text).

Integral variable change for the c field

In Eq. (11) we introduced a variable change that can alleviate the sign problem and reduce the statistical error. Here we demonstrate this point by comparing the results calculated without and with the variable change. In the upper panel of Fig. 3 we show the calculated transfer matrix energy

$$E_M = -\frac{1}{a_t} \ln \frac{\langle \Psi_T | M | \Psi_T \rangle}{\langle \Psi_T | \Psi_T \rangle} = -\frac{1}{a_t} \ln \frac{\int \mathcal{D}s \mathcal{D}c P(s) P(c) \langle \Psi_T | M(s, c) | \Psi_T \rangle}{\langle \Psi_T | \Psi_T \rangle}, \quad (15)$$

where M is the full transfer matrix corresponding to the full N²LO chiral interaction Eqs.(14) in the main text, s and c represent the auxiliary fields from decomposing the interactions. We take ¹⁶O as an example and $|\Psi_T\rangle$ is a shell model wave function (see below). The circles denote the results calculated by sampling the s and c field directly with a standard normal distribution, while the squares show results obtained with the variable change. We see that the latter calculation converges much faster. We also show the statistical errors in the lower panel. In both cases the errors decrease according to the theoretical scaling law $\Delta E \propto N^{-1/2}$ with N the number of measurements. With the variable change, however, the statistical errors are about one order of magnitude smaller.

The zeroth order SU(4) Hamiltonian

In the main text we use a zeroth order Hamiltonian that respects the Wigner-SU(4) symmetry. The details and parametrization can be found in Ref.[1]. For completeness we also present the details here. On a periodic L^3 cube with lattice coordinates $\mathbf{n} = (n_x, n_y, n_z)$, the Hamiltonian is

$$H_0 = K + \frac{1}{2} C_{\text{SU4}} \sum_{\mathbf{n}} : \tilde{\rho}^2(\mathbf{n}) :, \quad (16)$$

where K is the kinetic energy term with nucleon mass $m = 938.92$ MeV and the $::$ symbol indicate normal ordering. The

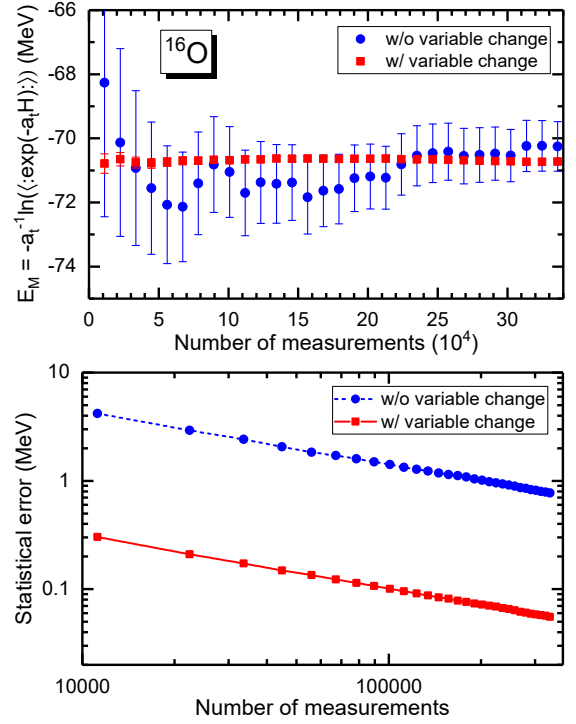


Figure 3. (Upper panel) Calculated transfer matrix energies E_M as functions of the number of measurements. The circles (blue) and squares (red) denote the calculations without and with the variable shift. (Lower panel) The corresponding statistical errors.

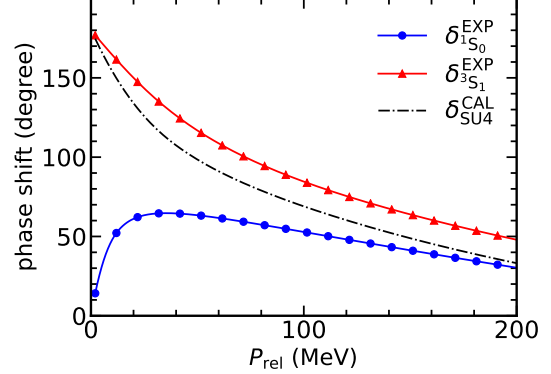


Figure 4. The triangles (red) and circles (blue) denote the empirical 1S_0 and 3S_1 phase shifts, respectively [2]. The dash-dotted curve represents the results from the zeroth order Hamiltonian Eq. (16).

smear density operator $\tilde{\rho}(\mathbf{n})$ is defined as

$$\tilde{\rho}(\mathbf{n}) = \sum_i \tilde{a}_i^\dagger(\mathbf{n}) \tilde{a}_i(\mathbf{n}) + s_L \sum_{|\mathbf{n}'-\mathbf{n}|=1} \sum_i \tilde{a}_i^\dagger(\mathbf{n}') \tilde{a}_i(\mathbf{n}'), \quad (17)$$

where i is the joint spin-isospin index and the smeared annihilation and creation operators are defined as

$$\tilde{a}_i(\mathbf{n}) = a_i(\mathbf{n}) + s_{NL} \sum_{|\mathbf{n}'-\mathbf{n}|=1} a_i(\mathbf{n}'). \quad (18)$$

The summation over the spin and isospin implies that the interaction is SU(4) invariant. The parameter s_L controls the strength of the local part of the interaction, while s_{NL} controls the strength of the non-local part of the interaction. Here we include both kinds of smearing. Both s_L and s_{NL} have an impact on the range of the interactions. The parameter C_{SU4} gives the strength of the two-body interactions. In this work we use a lattice spacing $a = 1.32$ fm and the parameter set $C_{SU4} = -3.41 \times 10^{-7} \text{ MeV}^{-2}$, $s_L = 0.061$ and $s_{NL} = 0.5$. These parameters together with a properly chosen three-body force can reproduce the binding energies and charge density distributions of light nuclei from ${}^3\text{H}$ to the Ca isotopes [1]. In Fig. 4 we show the NN S -wave phase shifts calculated with Eq. (16) (dash-dotted line) compared with the empirical 1S_0 (circles) and 3S_1 (triangles) phase shifts.

Construction of the N²LO chiral interaction

In this section we present the details of the nuclear chiral interaction used in the main text. Recently we have built a next-to-next-to-next-to-leading-order (N³LO) chiral interaction on the lattice, where all 24 low-energy constants (LECs) are determined by fitting to the empirical partial wave phase shifts and mixing angles [3] based on the improved spherical wall method [4]. These interactions are non-local and difficult to realize efficiently using auxiliary fields. In this work we employ another set of semi-local contact operators, which is completely equivalent to the non-local operators in Ref. [3] for two-body scattering. We note that similar constructions have already been used for the Green's function Monte Carlo calculations [5]. The local operator basis used here contains isospin dependent terms proportional to $\tau_1 \cdot \tau_2$. The results are given in Eq. (14). In this form, these operators can be written as products of one-body density operators and decomposed using auxiliary field transformations.

For 2N contact terms we introduce an extra non-local regulator $f_{2N} = \exp[-\sum_{i=1}^2 (p_i^6 + p_i'^6)/\Lambda^6]$, with $\Lambda = 340 \text{ MeV}$. Similarly, the OPEP in the last line of Eq.(14) is regulated with a local exponential regulator $f_\pi(q^2) = \exp[-(q^2 + M_\pi^2)/\Lambda_\pi^2]$ with $\Lambda_\pi = 300 \text{ MeV}$. The cutoffs are chosen to satisfy $\Lambda, \Lambda_\pi \ll \pi/a$ so as to minimize the lattice artifacts. We also tested other choices of the cutoffs and found similar results as presented here. For N²LO calculations in this work we fit the LECs to the Nijmegen phase shifts [2] below $P_{\text{rel}}=200 \text{ MeV} < 2M_\pi$. In this momentum interval the two-pion exchange potential can be approximately absorbed into the contact terms and discarded.

Besides the short-range contact terms, we also need a long-range one-pion-exchange potential (OPEP). Recently a semi-local momentum space regularized chiral potential was developed up to fifth order [6]. This regularization method is more convenient than other choices for lattice simulations. The OPEP we used is given in the last line of Eq. (14). The

constant C'_π is defined as

$$C'_\pi = \frac{1}{3\Lambda_\pi^3} \left[\Lambda_\pi (\Lambda_\pi^2 - 2M_\pi^2) + 2\sqrt{\pi} M_\pi^3 \exp\left(\frac{M_\pi^2}{\Lambda_\pi^2}\right) \text{erfc}\left(\frac{M_\pi}{\Lambda_\pi}\right) \right].$$

The term proportional to C'_π is a counterterm introduced to remove the short-range singularity from the OPEP [6]. We note that the OPEP regulated in this way is soft and adaptive to perturbative calculations. This can be clearly seen by comparing the contribution of the OPEP $\langle V_{\text{OPEP}} \rangle$ with the total potential energy $\langle V_{2N} + V_{3N} + V_{\text{cou}} \rangle$. Taking ${}^{16}\text{O}$ as an example, in this work we find $\langle V_{\text{OPEP}} \rangle = -18.9 \text{ MeV}$, which is more than one order smaller than the total potential energy -361.1 MeV . Thus we expect a fast convergence for the perturbative calculations including the OPEP. In section F below we will numerically demonstrate this point with the deuteron.

For the three-body force at N²LO we adopt a simple 3N contact term with Wigner SU(4) symmetry,

$$V_{3N} = \frac{c_E}{2F_\pi^4 \Lambda_\chi} f_{3N}(p_1, p_2, \dots, p_3), \quad (19)$$

where $\Lambda_\chi = 700 \text{ MeV}$ is the chiral symmetry breaking scale, $F_\pi = 92.2 \text{ MeV}$ is the pion decay constant, c_E is the coupling constant, $f_{3N} = \exp[-\sum_{i=1}^3 (p_i^6 + p_i'^6)/\Lambda^6]$ is a separable non-local regulator. In this work we use the same cutoff $\Lambda = 340 \text{ MeV}$ for both 2N and 3N interactions.

Besides the nuclear force we also include a Coulomb force. With lattice notations we write

$$V_{\text{cou}} =: \frac{\alpha}{2} \sum_{\mathbf{n}_1 \mathbf{n}_2} f_c(\mathbf{n}_1 - \mathbf{n}_2) \rho_p(\mathbf{n}_1) \rho_p(\mathbf{n}_2) : \quad (20)$$

where ρ_p is the total proton density. The fine structure constant $\alpha = 1/137$ and the function $f_c = 1/\max(|\mathbf{n}_1 - \mathbf{n}_2|, 1/2)$ give the regularized Coulomb force.

For a complete calculation, we should also include the long-range three-body forces from pion-exchange diagrams. However, these terms have only a minor impact on the main computational analysis of this study and so is reserved for future work. In V_{2N} and V_{3N} , we regulate the single particle momenta instead of the relative Jacobi momenta. These forms are more convenient to implement on the lattice but violate Galilean invariance. Nevertheless, the leading order Galilean breaking effect occurs at $\mathcal{O}((Q/\Lambda)^6)$ and will not be considered in the N²LO calculations presented here.

We determine the LECs B_i , C_i and c_E by fitting to the low-energy NN phase shifts, mixing angles and triton energy. The method is based on Ref. [4]. We decompose the scattering waves on the lattice into different partial waves, then employ the real and complex auxiliary potentials to extract the asymptotic radial wave functions. We follow the conventional procedure for fitting the LECs in the continuum [7]. We first determine the spectroscopic LECs for each partial wave, then the B_i and C_i can be obtained by solving the linear equations. In Table II we show the fitted LECs at NLO for cutoff $\Lambda = 340 \text{ MeV}$. At this order we consider NN scattering up to a relative momentum $P_{\text{rel}} = 200 \text{ MeV}$. Here we use the lattice unit

Table II. Fitted LECs at $N^2\text{LO}$ with $\Lambda = 340$ MeV and $\Lambda_\pi = 300$ MeV (dimensionless).

LEC	B_1	B_2	C_1	C_2	C_3
	-2.443	-0.125	0.143	-0.012	-0.013
LEC	C_4	C_5	C_6	C_7	c_E
	-0.020	0.273	0.0	-0.078	0.712

system $\hbar = c = a = 1$ and all LECs are dimensionless. In Fig. 5 we show the calculated phase shifts. The dotted and dash-dotted lines denote the results at LO and NLO, respectively. The red dots with error bars are empirical values from the Nijmegen partial wave analysis (NPWA)[2].

We determine the three-body coupling constant c_E by fitting to the triton energy. In Fig. 6 we show the triton energy calculated with the NLO interactions with the parameters from Table II as blue circles. We find that the experimental triton energy $E(^3\text{H}) = -8.482$ MeV can be reproduced with $c_E = 0.712$ at infinite volume. The corresponding results are shown as red diamonds. All results for the triton are obtained by exactly diagonalizing the lattice Hamiltonian using sparse matrix algebra.

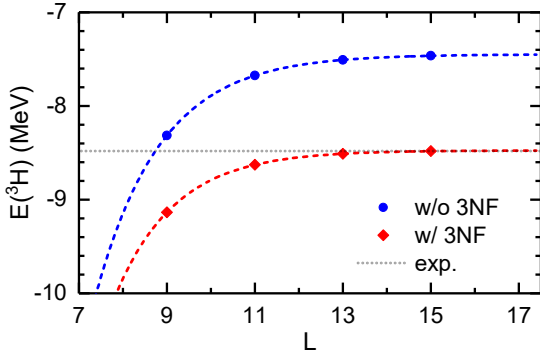


Figure 6. Triton binding energies as functions of the box size L . The circles (blue) and diamonds (red) denote the calculations without and with the three-body force, respectively. Horizontal line denotes the experimental value $E = -8.482$ MeV.

Trial wave functions

In this work the ^3H nucleus was always solved exactly with the sparse matrix algebra. The other nuclei from ^4He are simulated with the imaginary time projection method. The projection method requires properly chosen trial wave function that have large overlap with the exact ground state. We have tested different choices of the trial wave functions and found that the clustering states is best suited for nuclei lighter than ^{16}O . For ^{16}O a shell model wave function works better.

On the lattice the clustering state writes as the anti-symmetrized product of the single particle wave functions

$$\psi_i(\mathbf{r}, s, t) = \exp\left[-\frac{(\mathbf{r} - \mathbf{R}_i)^2}{2c^2}\right] \chi_i \zeta_i,$$

where $c = 1.4$ fm, χ and ζ are spin and isospin spinors, respectively. For first four nucleons with different spins and isospins we take $\mathbf{R}_i = (0, 0, 0)$ in lattice unit, and for next four nucleons we take $\mathbf{R}_i = (0, 0, 1)$, and so on. Then the nucleons form a compact configurations consisting of α -clusters centered around the origin. In Monte Carlo simulations we randomly move the positions of these α -clusters to form state with zero total angular momentum and zero total momentum.

The shell model wave function is the anti-symmetrized product of the harmonic oscillator wave functions

$$\psi_i(\mathbf{r}, s, t) = R_{n_r}^L(r) \vec{Y}_{JM}^L(\Omega) \zeta_i,$$

where the right-hand side is the solution of the Schrodinger equation in a harmonic oscillator with frequency $\hbar\omega = 41A^{-1/3}$ MeV. The spins have been coupled with the spatial angular momenta to form the spinor wave function \vec{Y}_{JM}^L . For closed shell nucleus ^{16}O the nucleons are injected from the bottom until the p -shell is filled up. The total angular momentum is automatically coupled to zero. In Monte Carlo simulations we also randomize the center of the harmonic oscillator to form state with zero total momentum.

Note that the full Hamiltonian is translational and rotational invariant and the exact ground state has zero total momentum P and angular momentum J . The projections to $P = 0$ and $J = 0$ increase the overlap of the trial wave function with the exact ground state and accelerate the convergence.

Imaginary time extrapolation

In Fig. 1 we performed extrapolations $\tau \rightarrow \infty$ to find the ground state energies. We found that both zeroth and second order energies can be well fitted by a decaying exponential function $E(\tau) = E(\infty) + C'e^{-\tau\Delta}$, where $E(\infty)$, C' and Δ are fitting parameters. We note that Δ has the physical meaning of the lowest excitation energy. On the contrary, the first order energies contain two decaying functions $E(\tau) = E(\infty) + C'e^{-\tau\Delta} + C''e^{-\tau\Delta/2}$, where the last term comes from the expectation value of V_C in $|\Psi_0\rangle$.

In Fig. 1 we observed that the first order energy E_1 are not a monotonically decreasing function of τ . The reason is that E_1 is the expectation value of the full Hamiltonian H in the zeroth order wave function $|\Psi_0\rangle$,

$$E_1(\tau) = \frac{\langle \Psi_T | e^{-\tau H_0/2} (H_0 + V_C) e^{-\tau H_0/2} | \Psi_T \rangle}{\langle \Psi_T | e^{-\tau H_0} | \Psi_T \rangle}. \quad (21)$$

For large τ only the ground state and first excited state of H_0 is relevant. We can approximately write

$$e^{-\tau H_0/2} | \Psi_T \rangle \rightarrow C e^{-\tau E_0/2} \left[| \Psi_0 \rangle + C' e^{-\tau\Delta/2} | \Psi'_0 \rangle \right] \quad (22)$$

where C and C' are certain constants of order $\mathcal{O}(1)$, the symbols with primes are that for the first excited state of H_0 , Δ is the excitation energy. Substituting Eq. (22) into Eq. (21) and use $\langle \Psi_0 | \Psi'_0 \rangle = 0$, $\langle \Psi_0 | \Psi_0 \rangle = \langle \Psi'_0 | \Psi'_0 \rangle = 1$, we find

$$E_1(\tau) = [E_0 + e^{-\tau\Delta} |C'|^2 E_1 + \langle \Psi_0 | V_C | \Psi_0 \rangle]$$

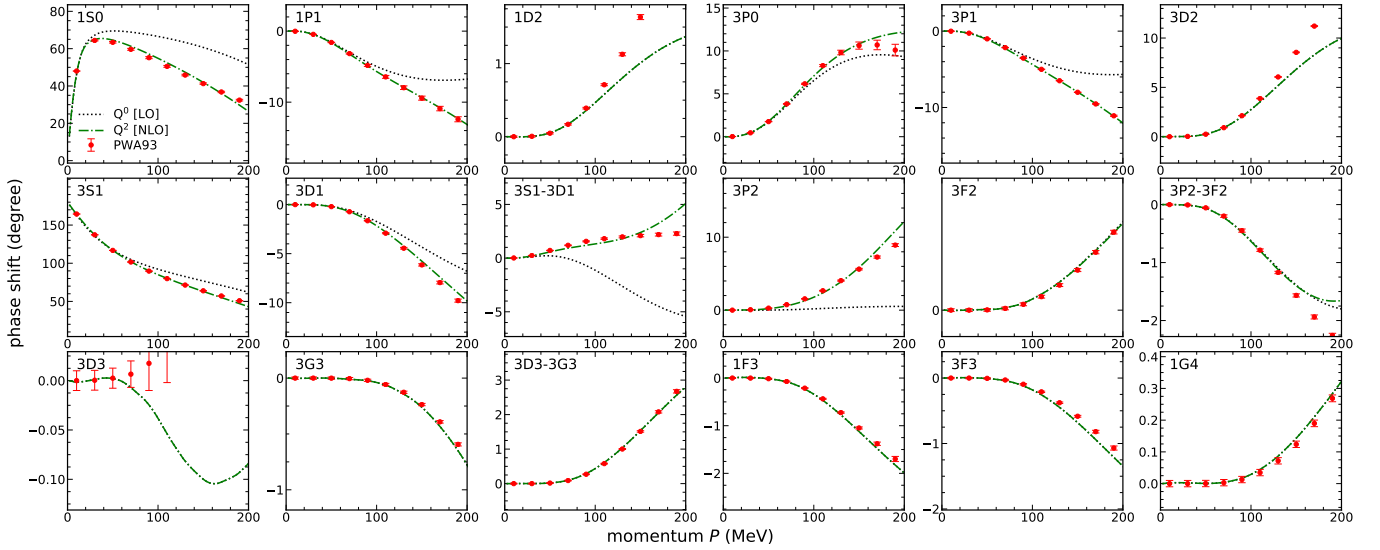


Figure 5. Calculated phase shifts for the LECs in Tab. II. Dotted and dash-dotted lines denote the LO and NLO results, respectively. Red circles with error bars show the empirical values [2].

$$\begin{aligned}
& +2e^{-\tau\Delta/2}\text{Re}[C'\langle\Psi_0|V_C|\Psi_0\rangle] \\
& +|C'|^2e^{-\tau\Delta}\langle\Psi'_0|V_C|\Psi'_0\rangle / (1 + |C'|^2e^{-\tau\Delta}) \\
= & E_0 + \langle\Psi_0|V_C|\Psi_0\rangle \\
& +e^{-\tau\Delta/2} \times 2\text{Re}[C'\langle\Psi_0|V_C|\Psi_0\rangle] \\
& +e^{-\tau\Delta}|C'|^2(E'_1 - E_1)
\end{aligned} \quad (23)$$

where we omitted the terms decaying faster than $e^{-\tau\Delta}$. $E_1 = \langle\Psi_0|H|\Psi_0\rangle$ and $E'_1 = \langle\Psi'_0|H|\Psi'_0\rangle$ are first order energies of the ground state and the excited state, respectively. The last term in $E_1(\tau)$ is positive and produces the usual exponential decay. However, the term proportional to $e^{-\tau\Delta/2}$ comes from the matrix element of V_C and is not positive definite. It decays slower and determines the behaviour of $E_1(\tau)$ at large τ . To see this point more clearly, in Fig. 7 we examine the first energy correction E_1 of ^{16}O in more detail. Here we plot the fitting function $E_1(\tau)$ as a solid line, then show the results with one of the two decaying functions removed separately. We see that the $e^{-\tau\Delta}$ term decays much faster and approaches a constant for large τ , while the $e^{-\tau\Delta/2}$ term dominates the asymptotic behaviour for $\tau > 0.1$. As shown in Eq. (23), the latter term might be negative and results in an increasing function at large τ . The summation of the two exponentials makes the first order energy decrease first and increasing later, and their cancellation results in a seemingly fast convergence for $\tau < 0.1$. However, this convergence is fictitious and we need to make the extrapolation more carefully.

On the other hand, the zeroth order energy $E_0(\tau)$ is simply Eq. (23) with V_C set to zero. The term proportional to $e^{-\tau\Delta/2}$ thus vanishes and we are left with a simple single decaying exponential function. Further, as we show in the main text that E_2 is a good approximation of the exact energy. Its dependence on τ is again determined by a single exponential function. We note that the simple behaviour of $E_2(\tau)$ can be

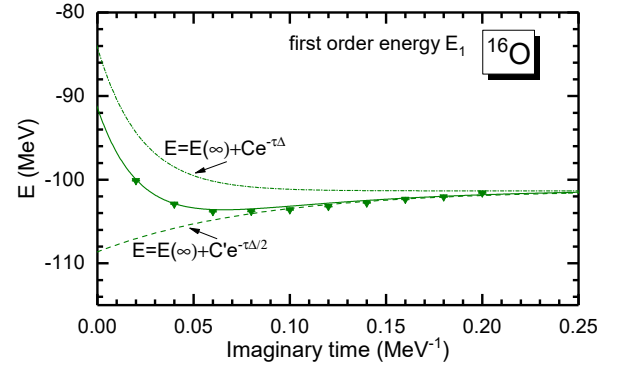


Figure 7. First energy correction E_1 for ^{16}O (down triangles). The solid line denotes the fitted result with two decaying exponential functions. The dashed and dot-dashed lines denote the results with one of the fitting exponential functions removed.

seen as a demonstration of the ptQMC method. If the perturbative corrections are not computed correctly, E_2 will contain more complex functions of τ , such as that we see in E_1 .

In fitting the energies we feed the statistical errors from the Monte Carlo simulations into the Levenberg-Marquardt algorithm. The resulting uncertainties of the extrapolated energy $E(\infty)$ are adopted as the errors shown in Fig. 2 and Table I.

Convergence of perturbation series beyond second order

In this section we examine the perturbative series beyond second order using the deuteron as an example. For the deuteron we can solve the Schrödinger equation exactly and find the perturbative corrections up to very high orders. Here we use the same Hamiltonians H and H_0 as used in the

main text. By extrapolating to infinite box size L , we find $E(^2\text{H}) = -2.28$ MeV for the chiral interaction used in this work, in good agreement with the experimental value $E_{\text{exp}} = -2.22$ MeV and within the expected truncation error of the chiral expansion in this order. As the deuteron binding energy is small, the continuum threshold plays an important role, and the convergence of perturbation theory is not the same as for nuclei with greater binding per nucleon. Thus we will consider a small periodic box $L = 5$, for which we have $E(^2\text{H}) = -7.733$ MeV. Note that the binding energy per nucleon for medium-mass nuclei is also of this order.

We calculate the eigenvalues of the Hamiltonian

$$H = (K + \mu V_0) + (V_{2N} + V_{\text{OPEP}} - \mu V_0), \quad (24)$$

where the symbols are the same as in the main text. Here μ is a real constant inserted as an analysis tool. We calculate the term in $K + \mu V_0$ using non-perturbative algorithms and treat $V_{2N} + V_{\text{OPEP}} - \mu V_0$ as the perturbing interaction. To obtain the perturbative expansion precisely, we multiply a variable λ to the perturbing Hamiltonian and calculate the energy E as a function of λ . We can use a complex λ and calculate $E(\lambda)$ on a closed contour encircling $\lambda = 0$ by exact matrix diagonalization. In Fig. 8 we show the real and imaginary parts of $E(\lambda)$ as functions of the azimuth angle θ on a circle with the radius $r = 0.2$. With these results we can calculate the derivatives $E^{(n)}(\lambda)$ using Cauchy's formula,

$$E^{(n)}(0) = \frac{n!}{2\pi r^n} \int_0^{2\pi} E(re^{i\theta}) e^{-in\theta} d\theta, \quad (25)$$

which can be performed with discrete Fourier transform. Unlike the differentiation formulae, the integral formula Eq. (25) can be very accurate even for very large n . Here we take 200 points uniformly distributed on the circle and calculate the derivatives up to $n = 14$.

The energy can be written as a power series,

$$E(\lambda) = \sum_{n=0}^{\infty} \frac{E^{(n)}(0)}{n!} \lambda^n. \quad (26)$$

Now let us check the convergence pattern of this series. For the full chiral Hamiltonian we have $\lambda = 1$, and the energy correction at the n -th order is simply $\delta E_n = E^{(n)}(0)/n!$. In Fig. 9 we show the energy corrections at each order for six different unperturbed Hamiltonian corresponding to $\mu = 0.6, 0.8, \dots, 1.6$, respectively. We find large δE_n at the first three orders $n = 0, 1, 2$. For $n \geq 3$ the contributions are small and become negligible very quickly when we continue to higher orders. We see that even though second order correction δE_2 can be large due to symmetry breaking effects, the third and higher orders follow the normal convergence pattern.

Let $E^{(n)}$ be the partial sum of the perturbative energy corrections up to order n . In Fig. 10 we show E_n versus order n for several different zeroth order Hamiltonians. The quick convergence to the exact energy can be clearly seen. Though in some cases the second order energy E_2 still has a weak

dependence on μ , we find that for $\mu = 1.0$ the second order energy $E_2 = -7.80$ MeV is already very close to the exact value $E = -7.733$ MeV, and the third order correction is small. As shown in the main text, the dependence of the perturbative energies on the zeroth order Hamiltonian can be used as a diagnostic tool for convergence check. In Fig. 11 we show the total energy E_0, E_1 and E_2 calculated with different μ . We find that while E_0 and E_1 have a strong dependence on μ , we always find approximately the same second order energy E_2 from different zeroth order Hamiltonians and are close to the exact energy.

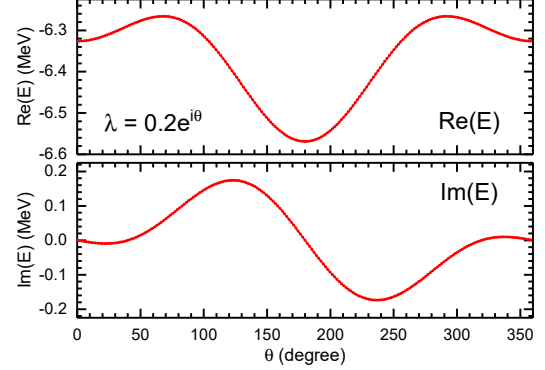


Figure 8. Deuteron energy as a function of the parameter θ . Calculated with $\mu = 1.0$.

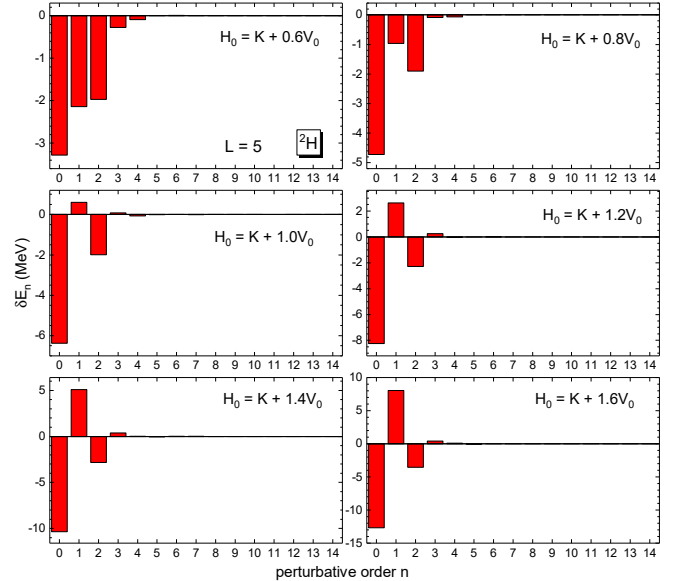


Figure 9. Perturbative energy correction δE_n of the deuteron at each order. For the zeroth order we show E_0 .

For the deuteron in a small periodic box, we conclude that while the second order correction is sizable due to symmetry-breaking perturbations, higher orders beyond second order are small. This is consistent with our findings for heavier nuclei in the main text. Our use of a relatively low momentum cutoff

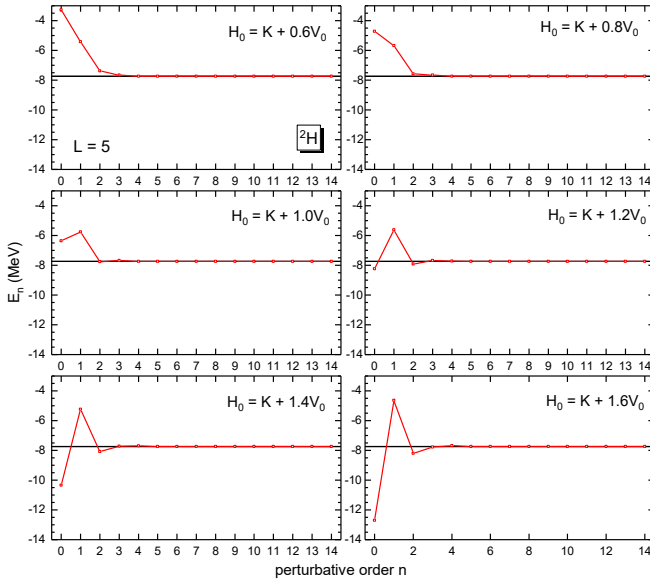


Figure 10. Partial energy sum E_n for the deuteron at each order. The black horizontal line is the exact energy.

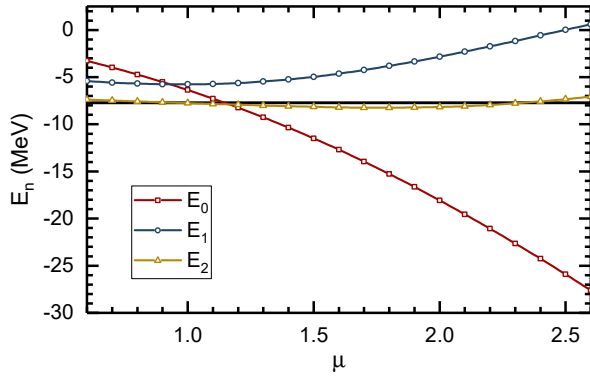


Figure 11. The zeroth, first and second order energies of the deuteron as functions of the parameter μ . The black horizontal line denotes the exact energy.

scale is likely playing an important role in keeping the size of the higher order corrections small.

For more general calculations, it is also possible that the higher orders have alternate signs and cancel with each other to give a small residual term. This usually occurs when the energy as a function of the small parameter λ has a singular point near the origin on the complex plane. For example, the

Taylor series of $f(\lambda) = 1/(1+\lambda)$ at $\lambda = 0$ has alternate signs near $\lambda = 1$ because it has a pole at $\lambda = -1$. It is well known that for two-body systems a pole or branch point appears when the bound state becomes a continuum state, thus it would be safe to apply the perturbation theory to deeply bound states as we do in this work.

Truncation errors

In the main text, we have discussed the case of ^{16}O and triangulated the binding energy. In this way, we could also obtain an estimate of the truncation error at the given order. Such an estimate can certainly be improved by referring to the underlying chiral expansion. A relatively easy way to improve on this uncertainty estimate would be the use of the method proposed in Ref. [8] and refined in Ref. [9]. More refined methods are based on Bayesian or bootstrap methods. For the former type of uncertainty quantification, we refer to the groundbreaking work in Refs. [10, 11], as applied e.g. to neutron-deuteron scattering at higher orders in the chiral EFT in Ref. [12].

* bnlv@giscaep.ac.cn

† lee.dean.j@gmail.com

‡ meissner@hiskp.uni-bonn.de

- [1] B.-N. Lu, N. Li, S. Elhatisari, D. Lee, E. Epelbaum, U.-G. Meißner, Phys. Lett. B 797, 134863 (2019)
- [2] V. G. J. Stoks, R. A. M. Klomp, M. C. M. Rentmeester, and J. J. de Swart, Phys. Rev. C48, 792 (1993).
- [3] N. Li, S. Elhatisari, E. Epelbaum, D. Lee, B.-N. Lu, U.-G. Meißner, Phys. Rev. C 98, 044002 (2018)
- [4] B.-N. Lu, T. A. Lähde, D. Lee, U.-G. Meißner, Phys. Lett. B 760, 309 (2016)
- [5] A. Gezerlis, I. Tews, E. Epelbaum, S. Gandolfi, K. Hebeler, A. Nogga, and A. Schwenk, Phys. Rev. Lett. 111, 032501 (2013)
- [6] P. Reinert, H. Krebs, E. Epelbaum, Eur. Phys. J. A 54, 86 (2018)
- [7] E. Epelbaum, W. Glöckle, U.-G. Meißner, Nucl. Phys. A 47, 362 (2005)
- [8] E. Epelbaum, H. Krebs and U.-G. Meißner, Eur. Phys. J. A 51, no.5, 53 (2015).
- [9] S. Binder *et al.* [LENPIC], Phys. Rev. C 93, no.4, 044002 (2016).
- [10] R. J. Furnstahl, N. Klco, D. R. Phillips and S. Wesolowski, Phys. Rev. C 92, no.2, 024005 (2015).
- [11] J. A. Melendez, S. Wesolowski and R. J. Furnstahl, Phys. Rev. C 96, no.2, 024003 (2017).
- [12] E. Epelbaum, J. Golak, K. Hebeler, H. Kamada, H. Krebs, U.-G. Meißner, A. Nogga, P. Reinert, R. Skibiński and K. Topolnicki, *et al.* Eur. Phys. J. A 56, no.3, 92 (2020).